Research Article

DE GRUYTER

Chuangmin Li, Zhuangzhuang Li*, Youwei Gan, and Qinhao Deng

Optimization and characterization of composite modified asphalt with pyrolytic carbon black and chicken feather fiber

https://doi.org/10.1515/rams-2023-0143 received June 16, 2023; accepted October 13, 2023

Abstract: Asphalt is a vital construction material for roads, and its properties can be enhanced by modification. In this study, a composite modified asphalt was developed using pyrolytic carbon black (PCB) and chicken feather fiber (CFF). Box-Behnken design of response surface methodology was employed to optimize the preparation parameters, and the optimal parameters were determined to be a PCB dosage of 15% (weight ratio), a CFF dosage of 0.3% (weight ratio), and a chicken feather (CF) shear time of 8.2 min. A Dynamic Shear Rheometer (MCR302) was used to analyze the high-temperature rheological properties of the modified asphalt samples, and the results showed that the addition of PCB and CFF enhanced the high temperature performance and anti-aging performance of the asphalt. The rheological properties at high temperature increased progressively with the increase in CFF dosage. The Bending Beam Rheometer (BBR) test was conducted to evaluate the low-temperature rheological property of PCB/CFF composite modified asphalt, which was observed to decrease with the increase in CFF dosage. The microscopic properties and the chemical group of 15% PCB + 0.3% CFF with 8.2 min CF shear time composite modified asphalt (0.3%PC-MA) were analyzed using Fourier Transform Infrared spectrometer and Fluorescence Microscopy, and the results indicated that PCB and CFF were physically blended with asphalt without

* Corresponding author: Zhuangzhuang Li, School of Traffic and Transportation Engineering, Changsha University of Science and Technology, Changsha 410114, China, e-mail: 20101030054@stu.csust.edu.cn

Chuangmin Li: School of Traffic and Transportation Engineering, Changsha University of Science and Technology, Changsha 410114, China; Key Laboratory of Road Structure and Material of Ministry of Transport (Changsha), Changsha University of Science and Technology, Changsha 410114, China

Youwei Gan, Qinhao Deng: School of Traffic and Transportation Engineering, Changsha University of Science and Technology, Changsha 410114, China undergoing a chemical reaction, and they were well compatible with and evenly distributed in asphalt. Finally, the high- and low-temperature performances, as well as water stability, of the base asphalt (BA), 15% PCB dosage modified asphalt (P-MA), and 15% PCB dosage modified asphalt with x% CFF dosage with a shear time of 8.2 min (PC-MA) were compared. The addition of CFF significantly enhanced the high-temperature and low-temperature performances, as well as water stability of P-MA mixtures. The aim of this study is to provide a laboratory test basis for the application of PCB/CFF composite modified asphalt.

Keywords: pyrolytic carbon black, chicken feather fiber, modified asphalt, rheological property, response surface methodology

1 Introduction

Automobiles have generated significant amounts of waste tires because of their rapid growth. It has been estimated that about 120 million waste tires will be generated worldwide by 2030 [1]. Compared with the treatment methods of refurbishing [2], regenerating rubber [3], and rubber powder [4], the thermal cracking method has the advantages of large processing capacity, no secondary pollution, and multiple resource recycling [2,5,6]. The main product is pyrolytic carbon black (PCB), which accounts for about 30% [7,8]. Due to the immature pyrolysis technology, the quality of PCB is poor, and the utilization rate of PCB is limited as well as low. For better utilization of PCB, some researchers have applied PCB to asphalt and obtained PCB modified asphalt, which is capable of improving pavement performance at high temperatures and anti-aging [9-11]. However, modified asphalt with more than 10% PCB dosage will be less resistant to cracking at low temperatures [12–14]. It also has adverse effects on water stability and uniform dispersion of modified asphalt [15]. Several scholars have modified PCB with other materials, including styrene-butadienestyrene (SBS) [16] and crosslinking agent [17], in order to

2 — Chuangmin Li et al. DE GRUYTER

enhance water stability and uniformity of modified asphalt with high dosages of PCB. Nevertheless, the disadvantages of these materials, such as complex production processes, high costs, and poor economy, do not meet the development trend of economic and environmental protection.

Not only industrial waste has potential in asphalt, but biological wastes can also play a great role in asphalt. Previous studies have shown that straw fiber [18], bagasse fiber [19], bamboo fiber [20], and areca nut fiber [21] can enhance asphalt properties, including high- and low-temperature properties, and increase their own recovery and utilization rate. At the same time, chicken feather (CF) is a by-product of poultry and chickens, which is characterized by high yield, low recovery, and heavy pollution [22,23]. Additionally, CF's shaft and barb differ from those of other natural or synthetic fibers. In addition to its flexibility, low density, and hollow structure, this protein fiber makes a good synthetic fiber [24]. In road engineering, chicken feather fiber (CFF) was first used to improve strength and durability properties of cement concrete [25], and later it was used in asphalt also. Rivera-Armenta [26] added CFF into asphalt and tested its performance at high temperatures against SBS modified asphalt. Based on the results, it was observed that CFF improved asphalt's high-temperature stability and helped it better resist permanent deformation. Furthermore, CFF improves the water stability of hot mix asphalt mixtures [27]. Additionally, experimental analysis of composites with CFF and other materials as asphalt modifiers concluded that CFF enhanced asphalt properties [29,30], proving the feasibility of using CFF and other materials as composite modifiers in asphalt. This study also confirmed that different fiber lengths have varying effects on asphalt modification. CFF is extracted by high-speed shear with a fixed rate of 39,000 rpm, so only the told shear time can affect the length of CFF. Therefore, different lengths of CFF can be obtained by changing the shear time of the high-speed multifunctional machine. As a result, it is crucial to find an appropriate fiber length [31,32]. Fiber length is generally controlled by its shear time.

In summary, the utilization of PCB-modified asphalt has demonstrated its ability to enhance pavement performance under high temperatures and provide anti-aging properties. However, the incorporation of PCB dosage beyond 10% in the modified asphalt mixture compromises its resistance to water damage, uniformity, and low-temperature performance. Alternatively, the integration of CFF in the modified asphalt offers advantages such as high flexibility, tensile strength, and a hollow network structure. These characteristics contribute to increased maximum breaking force and adhesion of the asphalt, while reducing temperature sensitivity, thus potentially improving the cracking resistance

and water stability of asphalt mixtures [27,28]. The preparation process and properties of PCB/CFF composite modified asphalt prepared by wet method were studied to provide a reference for improving the properties of PCB-modified asphalt mixture. An experimental design based on Box-Behnken design (BBD) of Response surface methodology (RSM) was employed to determine the optimal combination of independent variables, including PCB dosage, CFF dosage, and CF shear time. This evaluation encompassed key response variables including Penetration, Softening Point, Ductility, and 135°C Brookfield Viscosity indicators. Furthermore, an evaluation of the high-temperature and low-temperature rheological properties was conducted to assess the performance and structural properties of PCB/CFF modified asphalt. Microscopic analysis and the chemical groups, employing fluorescence microscopy (FM) and infrared spectroscopy, were performed to analyze the behavior of the PCB/CFF composite modified asphalt at a microscopic level. Comprehensive assessments of the performance of PCB/CFF composite modified asphalt were carried out through the preparation of asphalt mixtures, followed by testing under varying conditions, including high-temperature and lowtemperature performance, as well as water stability. The findings of this study offer valuable insights into the potential application of PCB/CFF composite as a modifier for asphalt mixtures.

2 Materials and methods

2.1 Materials

The test results of the technical indicators of 70 # matrix asphalt are shown in Table 1. PCB was produced by Qingdao, Shandong Province. Its technical indicators are listed in Table 2 and Figure 1. According to Figure 1, PCB particles are primarily sized between 0 and 10,000 nm. The D_{10} , D_{50} , and D_{90} of PCB were 197, 265, and 358 nm, sequentially, with an average of 307.3 nm.

Table 1: Asphalt technical index test results

Experiment	Specification limit	Value	Standard
Penetration (25°C, 0.1 mm)	60-80	68	ASTM D5
Softening point (°C)	≥46	48	ASTM D36
Ductility (10°C, cm)	≥15	37	ASTM D113
Ductility (15°C, cm)	≥100	>100	ASTM D113
Viscosity (135°C, Pas)	<3	0.731	ASTM D4402

Table 2: PCB technical index test results

Properties	Specification limit	Value	Standard	
Ash dosage (%)	≤18.5	14	JT/T860.7-2017	
Iodine absorption (mg·g ⁻¹)	≥80	81	GB/T 3780.1	
Oil absorption value (mL per 100 g)	≥70	76	GB/T 3780.2	
Moisture dosage (%)	≤3	2	JT/T 860.7-2017	
PH	≥6	8	GB/T 3780.7	

2.2 Pretreatment of CF

CFs were taken from a poultry breeding base in Changsha, Hunan Province. The technical characteristics of CFF are presented in Table 3. The sample preparation method followed the guidelines presented in a previous study [28]. The monofilament sample was elongated to achieve a straightened configuration and then securely attached to a paper frame using adhesive at both ends. This fixation process was performed meticulously, ensuring a consistent stretching rate of 2 mm·min⁻¹. The CF were pretreated, the collected CF were agitated and washed with detergent, and the debris was removed. The cleaned feathers were dried at 105°C and cooled to room temperature. A description of the CF processing is shown in Figure 2. Through many tests, it was found that when the shearing time was 3, 6, and 9 min, the obtained fiber length was about 9, 6, and 3 mm, respectively. Therefore, different shearing time is considered to replace the length of CFF. The high temperature resistance of CFF was tested with a thermogravimetric analyzer. Test condition: the temperature range is 30-800°C, and the heating rate is 5°C·min⁻¹. The test results are shown in Figure 3.

Mass loss ratio refers to the ratio of lost mass to initial mass. According to Figure 3, the mass loss of CFF was categorized into three major stages as the temperature increased. The first stage began at 43.83°C and ended at 80.3°C. The second stage began at 272.7°C and ended at 396.52°C. The third stage started from 396.52°C and continued until the end. The quality loss in the three stages was 7.881, 75.547, and 16.707% respectively. At first, the mass change of CFF was small, which was the loss of water evaporation. Then, with the increase in the temperature, more mass was lost and the CFF underwent thermal decomposition. Therefore, CFF could withstand the general asphalt mixture construction temperature.

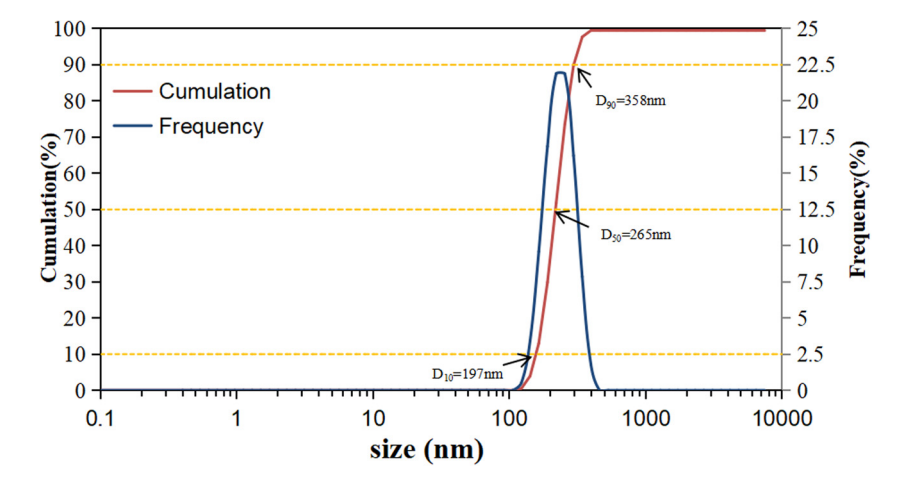


Figure 1: PCB particle size distribution.

Table 3: CFF physical property test results

Properties	Oil absorption ratio (%)	Water absorption (%)	Color change (210°C, 3 h)	рН	Ash content (%)	Specific gravity (g∙cm ⁻³)	Tensile strength (MPa)	Young's modulus (GPa)
Value	8.32	6.7	Color deepening	7.2	18	0.494	261	3.81



Figure 2: Preparation process of CFF.

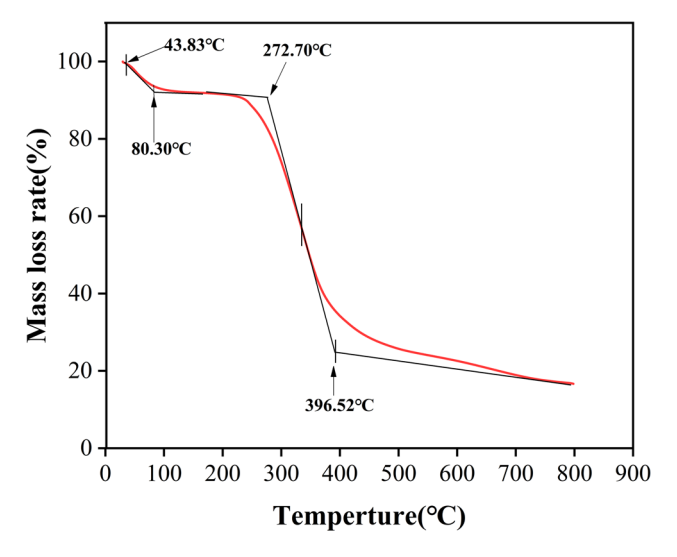


Figure 3: CFF thermogravimetric diagram.

2.3 Preparation of PCB/CFF composite modified asphalt

Based on previous studies [33,34], PCB/CFF composite modified asphalt was produced using constant temperature oil bath and high-speed shear machine. A description of the process is shown in Figure 4.

2.4 **RSM**

RSM is an analytical technique for optimizing a stochastic experimental process to study the quantitative correlation between independent and response variables [35], which incorporates random errors into the experiment. Meanwhile, the RSM could fit the unknown function relationship within a reasonable range using a simple polynomial model. This method is effective for solving practical problems, and it

produces a continuous prediction model. In comparison with orthogonal experiment, it has the advantage that all levels of the experiment could be analyzed continuously during optimization, whereas it is not possible to analyze all levels of an orthogonal experiment continuously during optimization. BBD test design is one of the common experimental design methods in RSM, and has the advantages of small test samples and low cost. Many scholars have applied the RSM in the field of road engineering [36,38]. The number of experimental groups in the BBD test design can be determined by Eq. (1). In this study, a total of 17 groups of experiments were designed according to the formula and factor level number, and 5 central points were designed to evaluate the random error.

$$N = 2k(k-1) + C_{\rm P},\tag{1}$$

where N is the number of tests; k is the number of factors; and C_p is the number of center points.

A BBD experimental design was used to investigate the PCB dosage, CFF dosage, and CF shear time of composite modified asphalt. Technical index of composite modified asphalt was adopted as response quantities to optimize the modifier dosage and CF shear time of composite modified asphalt. Three different levels of independent variables were selected according to the trend of asphalt technical indicators under different levels of independent variables. The levels and codes of each factor in the BBD test design are demonstrated in Table 4.

2.5 Test method

2.5.1 Conventional properties

The penetration value of the asphalt at 25°C after being penetrated with a 100 g standard needle for 5 s was measured in accordance with the specification (ASTM D5). In

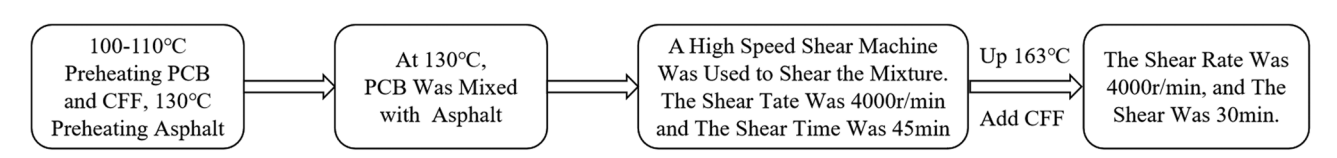


Figure 4: Production process of composite modified asphalt.

Table 4: BBD factor levels and coding

Level		Factors	
	A PCB dosage (%)	<i>B</i> CFF dosage (%)	C CF shearing time (min)
-1	5	0.3	3
0	10	0.6	6
1	15	0.9	9

the case of the softening point, the softening point of asphalt was the heating temperature at which the steel ball drops to a fixed depth (ASTM D36). The ring was filled with asphalt, and a 3.5 g steel ball was placed on its surface. The 10°C ductility of asphalt was measured following the ASTM D113. Meanwhile, the rotational viscometer (RV) was used to assess the workability for modified asphalt according to ASTM D4402. The test temperature and rotor type of the RV test were 135°C and the No. 27 rotor, respectively.

2.5.2 High-temperature rheological property

Temperature sweep was conducted on the following asphalt samples: original asphalt, asphalt subjected to Rolling Thin Film Oven Test (RTFOT) aging, and asphalt subjected to Pressure Aging Vessel (PAV) aging. The temperature sweep range was 46-82°C with a sweep interval of 6°C and the loading frequency was 10 rad·s⁻¹ (1.59 Hz), with a parallel plate spacing of 1 mm and a strain of 10%. Frequency sweep tests were performed using unaged asphalt of various asphalts. A 25 mm parallel plate was selected with a spacing of 1 mm, a load frequency range of 0.1–100 rad·s⁻¹, and a temperature range of 46-82°C, the temperature interval of 6°C, and the strain of 10%. Multiple stress creep recovery (MSCR) tests were performed on RTFOT aged asphalt at temperatures of 58, 64, and 70°C. The properties of different asphalts were analyzed by the obtained recovery rate (R) and non-recoverable creep compliance (I_{nr}) . Using temperature sweep tests, we investigated how temperature affected the rheological properties of asphalt. The frequency sweep test simulated different frequencies of vehicle speed to investigate how vehicle speed affected the rheological properties of asphalt. The MSCR was used to test the effect of repeatedly applying external force and its rutting resistance.

2.5.3 Low temperature rheological property

Standard trabecular specimens made from different asphalt after aging were put into a temperature-controlled aqueous

ethanol liquid bath in BBR. After being held at the prescribed temperature for 1 h, a consistent load lasting 240 s was applied in accordance with the operational procedure. Two parameters, creep stiffness (*S*) and creep rate (*m*), were obtained to assess the low-temperature rheological properties of the asphalt.

2.5.4 Textural characterization

Fourier Transform Infrared (FTIR) Spectrometer and FM were used for the chemical groups and micro structure of asphalt. FTIR measurements were conducted in 4,000–400 cm⁻¹ wavelength range and the sweeps were repeated 32 times to analyze whether functional group changes occurred during asphalt modification. Strong ultraviolet light was adopted in FM to irradiate the material and get the distribution of the material.

According to the above test content, this study's research process is shown in Figure 5.

3 Composite modified asphalt preparation parameters analysis

The outcomes of the BBD experimental design, conducted *via* the RSM employing Design Expert software, is documented in Table 5.

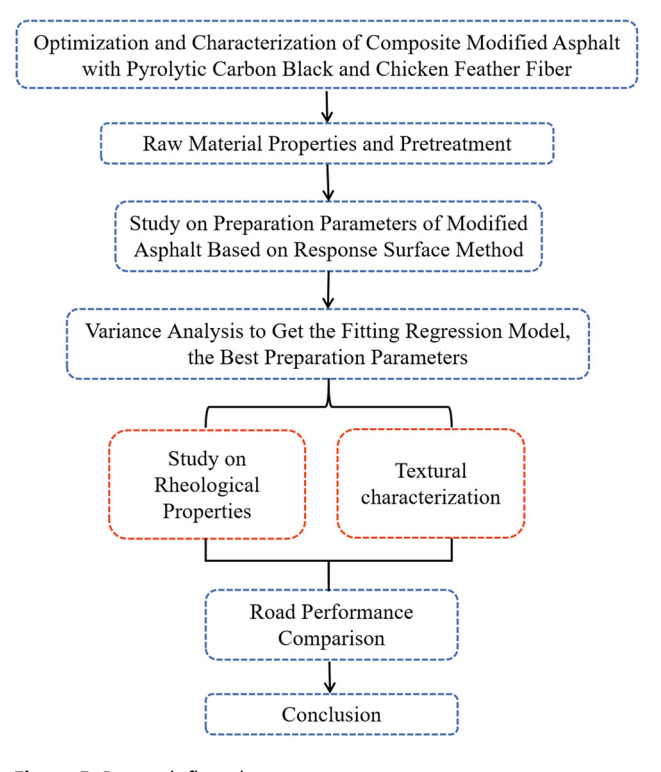


Figure 5: Research flow chart.

Table 5: BBD experimental design outcomes

Exp. no.	A (%)	B (%)	C (min)	Y ₁ (0.1 mm)	<i>Y</i> ₂ (°C)	Y ₃ (cm)	<i>Y</i> ₄ (Pa s)
1	15	0.6	9	52.1	54.9	10.2	1.815
2	5	0.6	3	57.6	53.9	13.1	2.306
3	10	0.6	6	56	52.9	12.6	1.966
4	5	0.6	9	57.5	52	13.5	1.816
5	10	0.6	6	55.8	53.3	12.9	1.855
6	15	0.3	6	54.2	55	12.8	1.318
7	5	0.9	6	55.1	54.9	13.2	2.591
8	10	0.6	6	55.6	53.1	12.4	1.902
9	5	0.3	6	59.9	51.8	15.6	0.937
10	10	0.6	6	55.5	53.1	12.8	1.944
11	10	0.3	9	56.9	52.4	13.9	0.973
12	10	0.3	3	56.3	52.8	13.8	1.784
13	15	0.6	3	53.4	55.5	9.6	2.541
14	10	0.9	3	52.7	55.9	9.4	2.778
15	10	0.9	9	52.3	54.7	12.3	2.319
16	15	0.9	6	51.1	56.2	9.2	2.455
17	10	0.6	6	55.1	53.4	12.4	1.876

3.1 Analysis of ANOVA

In the ANOVA analysis of this experiment, the *P* value was 0.05. A *P*-value of less than 0.05 indicates statistical significance, and *vice versa*. Since the four response measures were analyzed by the same process, the penetration analysis is used here to illustrate, whose statistics of penetration are described in Table 6.

According to Table 6, the *P*-value (<0.0001) < 0.05 of the penetration model showed that it was significant. The *P*-value for the loss of fit error for the insertion degree model (0.4916) > 0.05 indicated that the model was highly successful in fitting and could be used to better fit the data. The *P* values for the

Table 6: Results of the ANOVA analysis conducted for penetration

Source	Sum of squares	d _f	Mean square	<i>F</i> value	Prob > F (<i>P</i> -value)
Model	82.94	9	9.22	81.4	<0.0001
Α	46.56	1	46.56	411.27	<0.0001
В	32.40	1	32.4	286.19	<0.0001
С	0.18	1	0.18	1.59	0.2477
AB	0.7225	1	0.7225	6.38	0.0395
AC	0.36	1	0.36	3.18	0.1177
BC	0.25	1	0.25	2.21	0.1809
A^2	0.0059	1	0.0059	0.0523	0.8256
B^2	1.33	1	1.33	11.77	0.011
C ²	1	1	1	8.84	0.0207
Residual	0.7925	7	0.1132		
Lack of fit	0.3325	3	0.1108	0.9638	0.4916
Pure error	0.46	4	0.115		
Cor total	83.73	16			

single factor primary variables A and B, interaction variables AB, quadratic variables B^2 and C^2 were all less than 0.05, which were significant terms of the model, while the rest were not significant for the model.

3.2 Interaction analysis

Response surface is a three-dimensional spatial surface plot formed by the interaction of independent variables on the response quantity. The response surface diagram among three factors with different response quantities is analyzed below.

According to Figure 6, the penetration of composite-modified asphalt decreased with the increase in the PCB dosage. PCB, as a sub-micron particle, could be uniformly fused into the asphalt by high-speed shear, which hardened the asphalt and reduced the penetration. By increasing the CFF dosage, penetration decreased as well, but the degree of reduction was smaller compared with the PCB dosage. The grain size of CFF was larger than that of PCB, and its compatibility with asphalt was slightly poor. CFF was softer, affecting the hardness of asphalt less than PCB. When the CF shear time was changed, the penetration of composite-modified asphalt did not change. In accordance with the interaction surface diagram of penetration, in the pairwise interaction of three factors, PCB dosage dominated, followed by CFF dosage, and finally CF shear time.

According to Figure 7, the softening point of composite-modified asphalt increased with the increase in the PCB dosage and CFF dosage. As CF shear time increased,

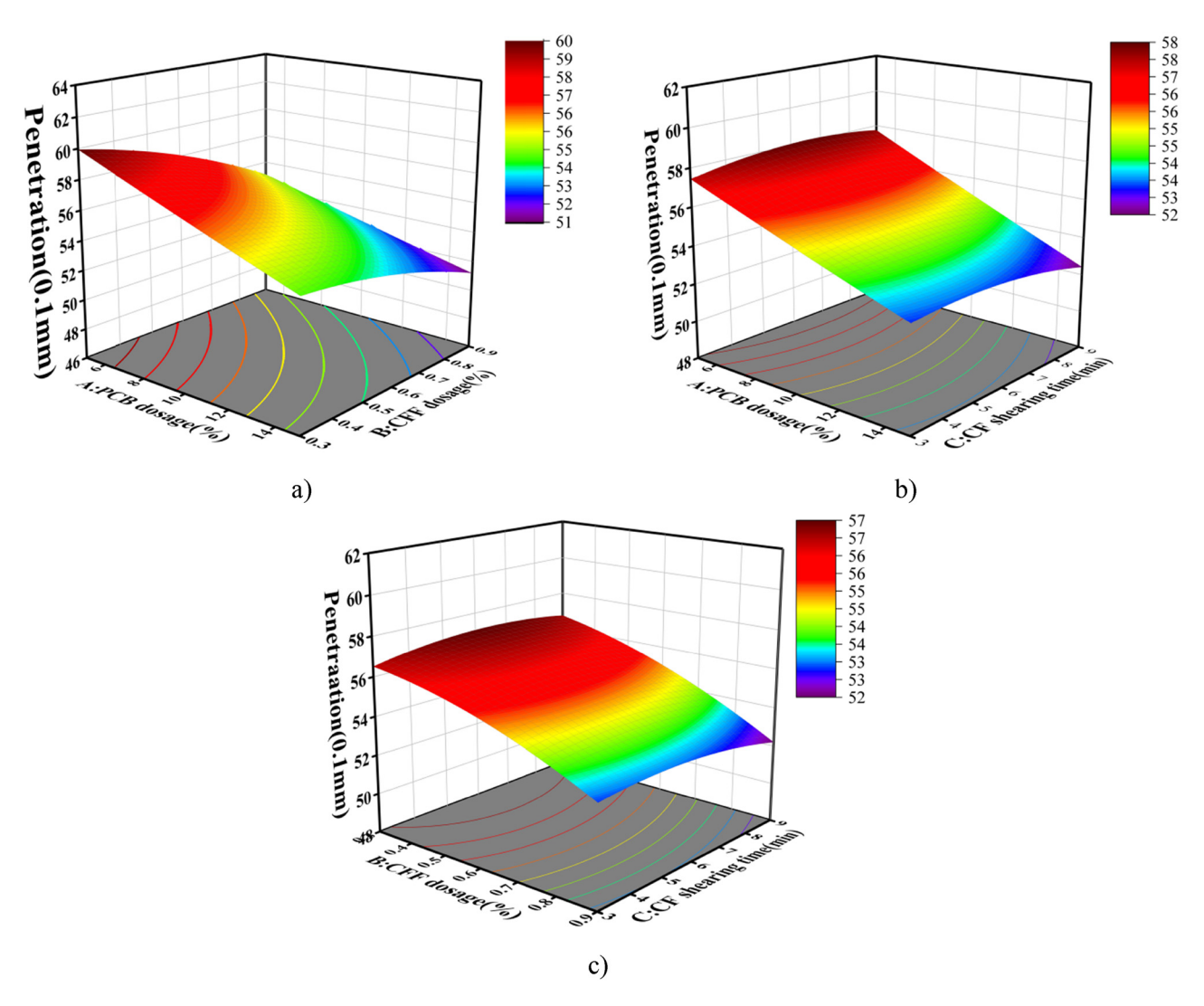


Figure 6: Response surface of penetration. (a) A vs B, (b) A vs C, and (c) B vs C.

the softening point increased, and then flattened. This revealed that there was a peak value of CF shear time, which could not be continuously increased. The CF shear time was shorter, the length of feather fibers was larger, and more likely to agglomerate, which was not conducive to its dispersion in asphalt and would lead to a large difference in softening points. As the shear time increased, the length of feather fibers became shorter and could be better dispersed in the asphalt, making the asphalt properties more balanced. The curvature of the surface graph between PCB dosage and CFF dosage, and PCB dosage and CF shear time was larger, and the contour line was close to the ellipse. The interaction between them was strong while the interaction between CFF dosage and CF shear time was weak. According to the softening point interaction surface plot, CFF dosage dominated among the pairwise interactions of the three factors, followed by PCB dosage and finally CF shear time.

According to Figure 8, the ductility of composite-modified asphalt decreased with the increase in the PCB dosage and CFF dosage. As the CF shear time increased, the ductility of the composite-modified asphalt initially increased before reaching a peak and subsequently decreased. With the change in shearing time, the length of feather fiber decreased, but its diameter did not change, so the length-diameter ratio of feather fiber would change accordingly. An appropriate length-diameter ratio could withstand greater tensile stress, making it less prone to fracture, thus there was an optimal value of CF shear time. Among the interaction effects of the three factors on the ductility, only the interaction between CFF dosage and CF shear time had a large curvature, and the contours were close to ellipses, so the interaction was obvious. The interaction of PCB dosage with CFF dosage and CF shear time was not obvious. According to the surface diagram of elongation interaction, PCB dosage dominated the pairwise

8 — Chuangmin Li et al. DE GRUYTER

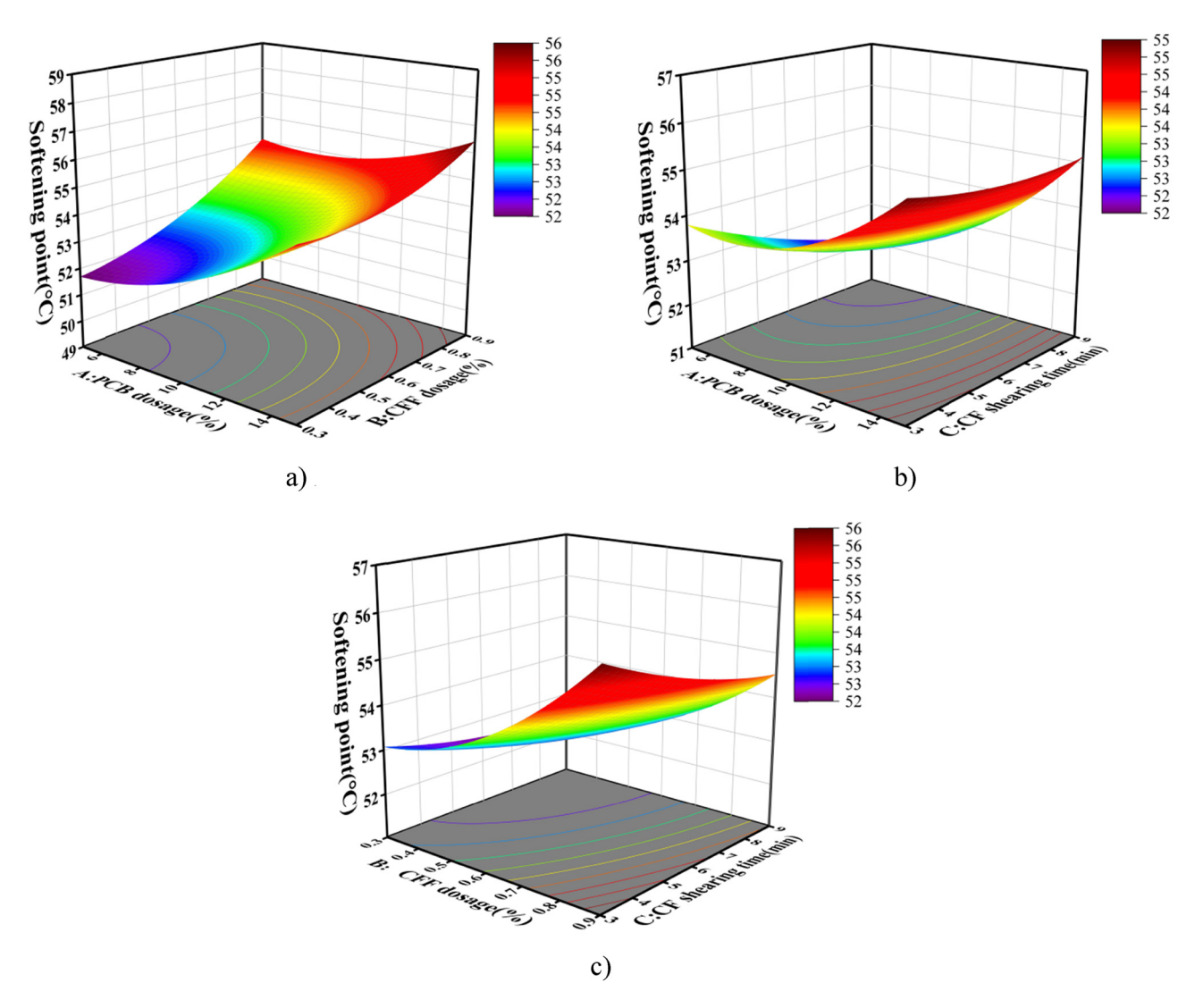


Figure 7: Response surface of softening point. (a) A vs B, (b) A vs C, and (c) B vs C.

interaction of the three factors, then the CFF dosage, and finally the CF shear time.

According to Figure 9, the viscosity of the composite modified asphalt increased with the increase in the PCB and CFF dosages. As the shear time of feather fibers increased, the viscosity increased, and then decreased. Longer feather fibers tended to clump together, making the asphalt thicker and more viscous. The short length of feather fibers was better dispersed in the asphalt, and their contact surface area increased, and their contact was more uniform. Among the interaction between the three influencing factors of viscosity, the curvature of PCB, CFF, and CF shear time surface graph were larger, and the contour line was close to the ellipse, and the interaction between PCB and CFF was higher than that between PCB and CF shear time, but the interaction between CFF and CF shear time

was not significant. According to the surface plot of the interaction of viscosity, the CFF dosage dominated the pairwise interaction of the three factors, followed by the CF shear time and finally the PCB dosage.

3.3 Response model establishment and analysis

Significant and insignificant items in the model fitting process were determined by ANOVA for each response. In order to make the obtained model more truly reflect practical problems, influential factors with *P* value greater than 0.05 could be deleted from the analysis of variance Tab, thus creating a simplified mode. The quadratic item model

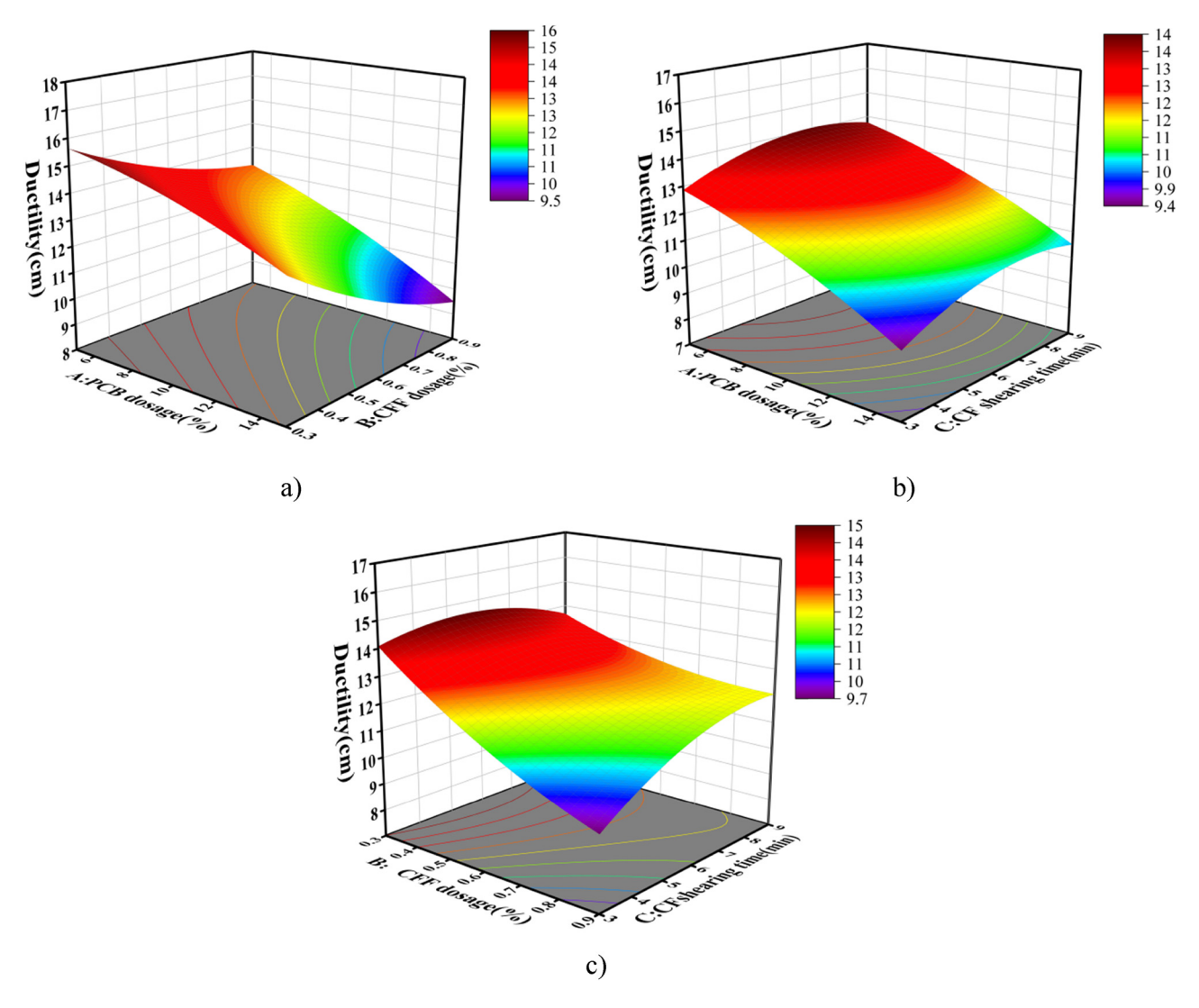


Figure 8: Response surface of ductility. (a) A vs B, (b) A vs C, and (c) B vs C.

obtained after eliminating non-significant items of each response quantity is displayed in Table 7.

Table 7 shows that the minimum and maximum values of \mathbb{R}^2 , adjusted \mathbb{R}^2 , and predicted \mathbb{R}^2 of each response quantity model are 0.8599 and 0.9878, which are close to 1, indicating that each response quantity model is well fitted. The Adeq. precision is proportional to the prediction R^2 , and the Adeq. precision of the fitting model is >4, suggesting that the model is accurate. The minimum Adeq. precision of the fitting model of each response quantity is 24.02 > 4, showing that it is able to accurately predict the results.

As can be seen from Figure 10, data points for the four response quantities are distributed along the diagonal line, indicating that the fitting model of the four response quantities is reasonable.

3.4 Optimization and verification of optimal preparation parameters

To achieve optimal performance of composite-modified asphalt, it is crucial to optimize the preparation parameters. With reference to the requirements [35], the target performance of each response quantity was determined. Optimal preparation parameters for composite modified asphalt with target performance were obtained using Design-Expert software, including PCB dosage of 15%, CFF dosage of 0.3%, and CF shear time of 8.2 min. Compared with literature [39], the PCB dosage was increased from 10 to 15%. The dosage of PCB in the PCB/CFF composite modified asphalt is 50% higher compared to that of single PCB modified asphalt. The results under the optimal preparation parameters were tested and verified. The results are presented in Tables 8 and 9.

10 — Chuangmin Li et al. DE GRUYTER

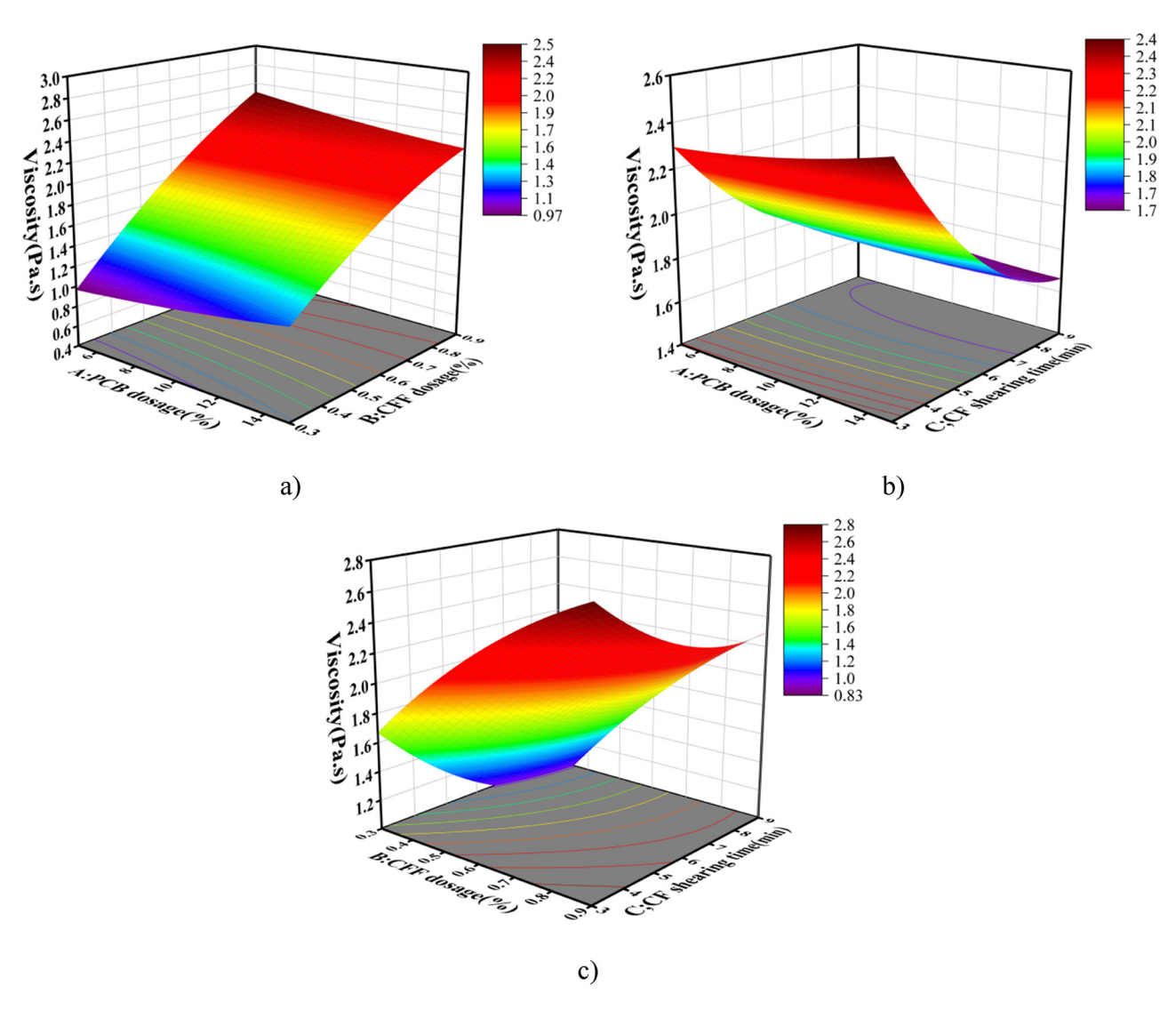


Figure 9: Response surface of 135°C Brookfield viscosity. (a) A vs B, (b) A vs C, and (c) B vs C.

Table 7: Simplified quadratic models of each response quantity

Responses	Quadratic reduced model	R ²	Adjusted R ²	Predicted R ²	Adeq. precision
<i>Y</i> ₁	$Y_1 = 62.282 - 0.653A - 2.068B + 0.597C + 0.283AB - 6.228B^2 - 0.054C^2$	0.9832	0.9731	0.9563	36.75
<i>Y</i> ₂	$Y_2 = 54.334 - 0.299A - 0.862B - 0.388C - 0.317AB + 0.022AC + 0.029A^2 + 6.725B^2$	0.9759	0.9571	0.8869	24.02
Y_3	$Y_3 = 19.458 - 0.34A - 14.965B + 0.637C + 0.778BC + 4.415B^2 - 0.078C^2$	0.9685	0.9496	0.8599	26.13
<i>Y</i> ₄	$Y_4 = 1.213 + 0.064A + 3.983B - 0.398C - 0.086AB + 0.098BC - 1.308B^2 + 0.02C^2$	0.9878	0.9784	0.9212	35.9

According to Table 9, under the optimal preparation parameters, there are some differences between the measured response value and the optimized predicted value, but the relative error is within the range. It shows that the model obtained by RSM has high fitting degree and certain reliability.

4 CFF dosage and rheological properties of asphalt

In order to identify the optimal preparation parameters for composite modified asphalt, rheological properties of base asphalt (BA), 15% PCB-modified asphalt (P-MA), and 15%

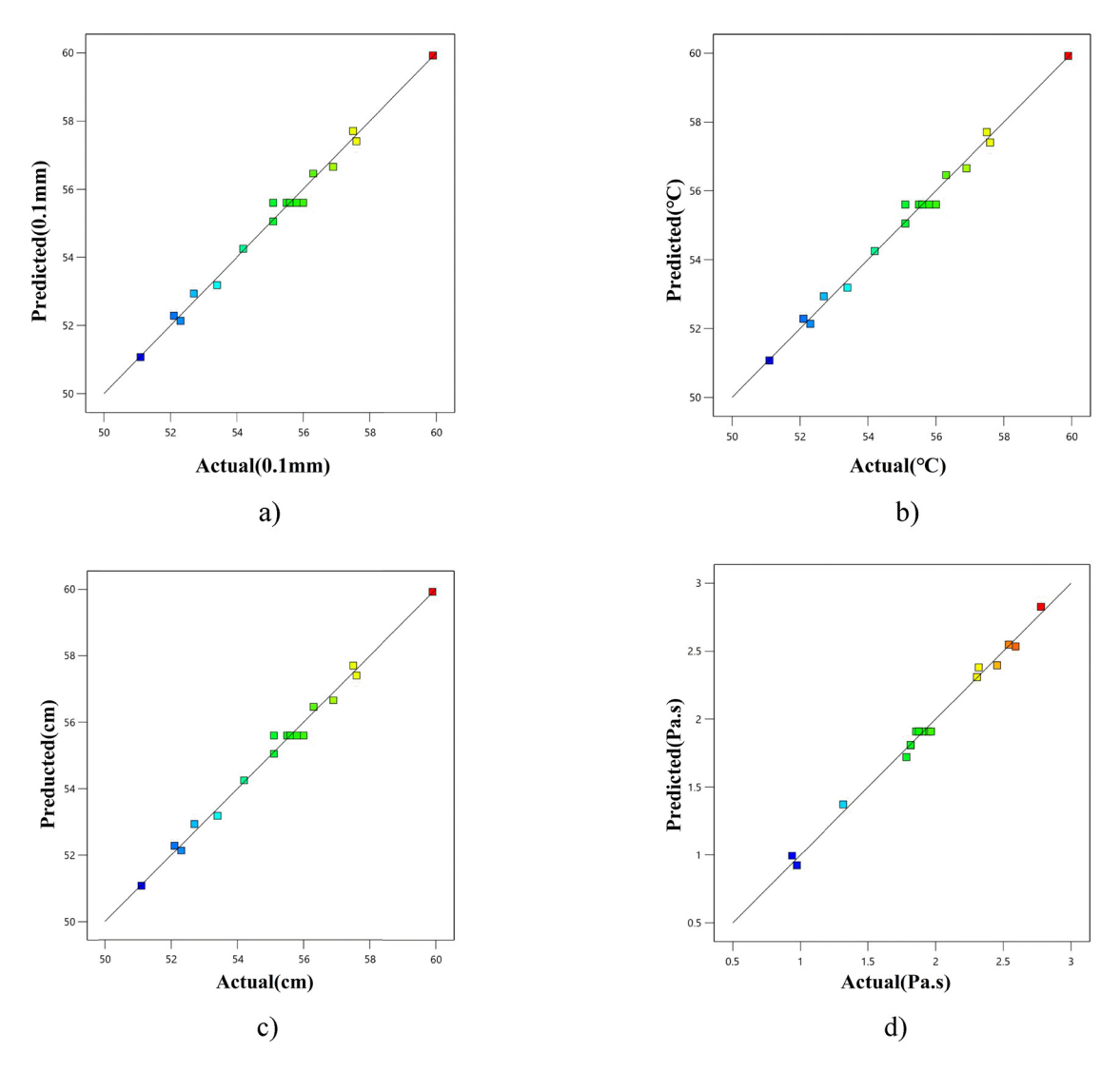


Figure 10: Comparison between model prediction and actual value of each response quantity. (a) Penetration, (b) softening Point, (c) ductility, and (d) 135°C Brookfield viscosity.

PCB modified asphalt with x% CFF dosage with a shear time of 8.2 min (x% PC-MA), were studied individually. The objective was to determine the impact of PCB and CFF dosage on the performance of asphalt at both high and low temperatures.

4.1 High temperature rheological property

A comparison of the results of temperature sweep of different asphalt types according to their aging are shown in Figure 11. According to Figure 11a, different asphalts' complex moduli decrease with the increase in the temperature. Because with the increase in temperature, asphalt gradually becomes a liquid fluid, the cohesion between asphalt molecules decreases, resulting in easier flow between asphalt molecules, more prone to deformation. Among them, when heated to the same level, BA has the lowest complex modulus, followed by P-MA, and 0.5%PC-MA is the highest, suggesting that PCB and CFF is beneficial in enhancing the high-temperature properties of asphalt. At the same temperature, the

Table 8: Optimization objectives of response values

Index	Penetration (0.1 mm)	Softening point (°C)	Ductility (cm)	135°C Brookfield viscosity (Pas)
Target	Min	Max	Max	Min

Table 9: Predicted values	of optimal preparation i	parameters and verified values

Туре	PCB dosage (%)	CFF dosage (%)	CF shearing time (min)	Penetration (0.1 mm)	Softening point (°C)	Ductility (cm)	135°C Brookfield viscosity (Pa s)
Predicted	15	0.3	8.2	51.1	55.9	11.9	1.136
Actual	15	0.3	8.2	52.1	56.1	14.6	1.187
	15	0.3	8.2	51.1	55.9	11.9	1.136
	15	0.3	8.2	52.9	54.4	13.5	1.22
Mean value				52	56.37	13.3	1.181
Error (%)				3.3	2.49	8.4	4.33

complex modulus of different asphalt types decreases in the following order: 0.5%PC-MA > 0.3%PC-MA > 0.1%PC-MA > P-MA > BA. According to Figure 11b, the phase angle of different bitumen increases with the increase in temperature. As the temperature increases, bitumen gradually becomes a flowing state and is more prone to shear deformation. Among them, at the same temperature, BA phase angle is the largest, followed by P-MA, and the phase angle between PC-MA is close, which is the smallest.

According to Figure 11c, as the temperature increased, the $G^*/\sin \delta$ showed a decreasing trend, and the decreasing trend was obvious before 58°C, and then the decreasing trend was slow and gradually smooth. This is because when the temperature rises, the elasticity will transform into viscosity. Before 58°C, the elasticity will transform into viscosity faster, and then it will slow down until the elasticity is completely transformed into viscosity. The lower the elasticity of asphalt, the worse its deformation resistance at high temperatures. By synthesizing Figure 11c-e, the $G^*/\sin \delta$ of asphalt gradually increases with aging, and the $G^*/\sin \delta$ of asphalt after long-term aging increases significantly, and the rutting resistance ability is the strongest. At the same temperature, the $G^*/\sin \delta$ values of all asphalt types follow the order of BA, P-MA, and PC-MA, with PC-MA having the highest value, indicating that the addition of PCB and CFF enhances the high-temperature performance of asphalt.

The processing method of frequency sweeping results of different bitumen is the same, so P-MA is used as an example to introduce the processing method of frequency sweeping results. P-MA frequency sweeping processing results are shown in Figure 12. According to Figure 12, the asphalt complex modulus—angular frequency relationship at different temperatures presents a certain linear relationship in logarithmic coordinate system. At the same angular frequency, complex modulus decreases with temperature. At the same temperature, complex modulus increases with angular frequency. The complex modulus increases when the frequency is larger, while the

temperature increases, the complex modulus decreases, so it can be obtained that the frequency and temperature are negatively correlated.

According to the P-MA composite mode—angular frequency fitting curve method, Williams-Landel-Ferry formula was used to calculate the displacement factors of different bitumen at different temperatures with 64°C as the reference temperature. The displacement factors are translated to the reference temperature, and the asphalt's main curve of complex modulus is shown in Figure 13.

According to Figure 13, the change trend of curves for complex modulus between different asphalts is basically the same, which increases with frequency. The more the dosage of modified additives in asphalt, the higher the main curve of its complex modulus, indicating that under the action of the same frequency, the more the dosage of additives, the larger the complex modulus, the better the resistance to shear deformation performance. According to the time-temperature equivalence principle, under the action of low frequency, the complex modulus of 0.5%PC-MA is the highest, so under high temperature conditions, 0.5%PC-MA has the best high temperature stability, followed by 0.3%PC-MA. However, the complex modulus of 0.3%PC-MA is similar to that of 0.5%PC-MA, indicating that the improvement effect becomes smaller with the increase in CFF dosage. The MSCR results for various asphalts can be seen in Figures 14 and 15.

According to Figure 14, under the two stress conditions, the *R*-values are 0.5%PC-MA, 0.3%PC-MA, 0.1%PC-MA, P-MA, and BA in the order from large to small, and the *R*-values of CFF with high dosage increase rapidly, indicating that construction of PCB and CFF can effectively enhance the anti-deformation ability of asphalt and strengthen the elasticity of asphalt. The R value of asphalt decreases as a function of temperature. Because in high temperature conditions, asphalt flows more easily, deformation resistance is weakened, and it is more prone to disease. At the same temperature, taking P-MA as an example, *R* value at 3.2 kPa at 58, 64, and 72°C decreased by 76, 90, and 95%, respectively.

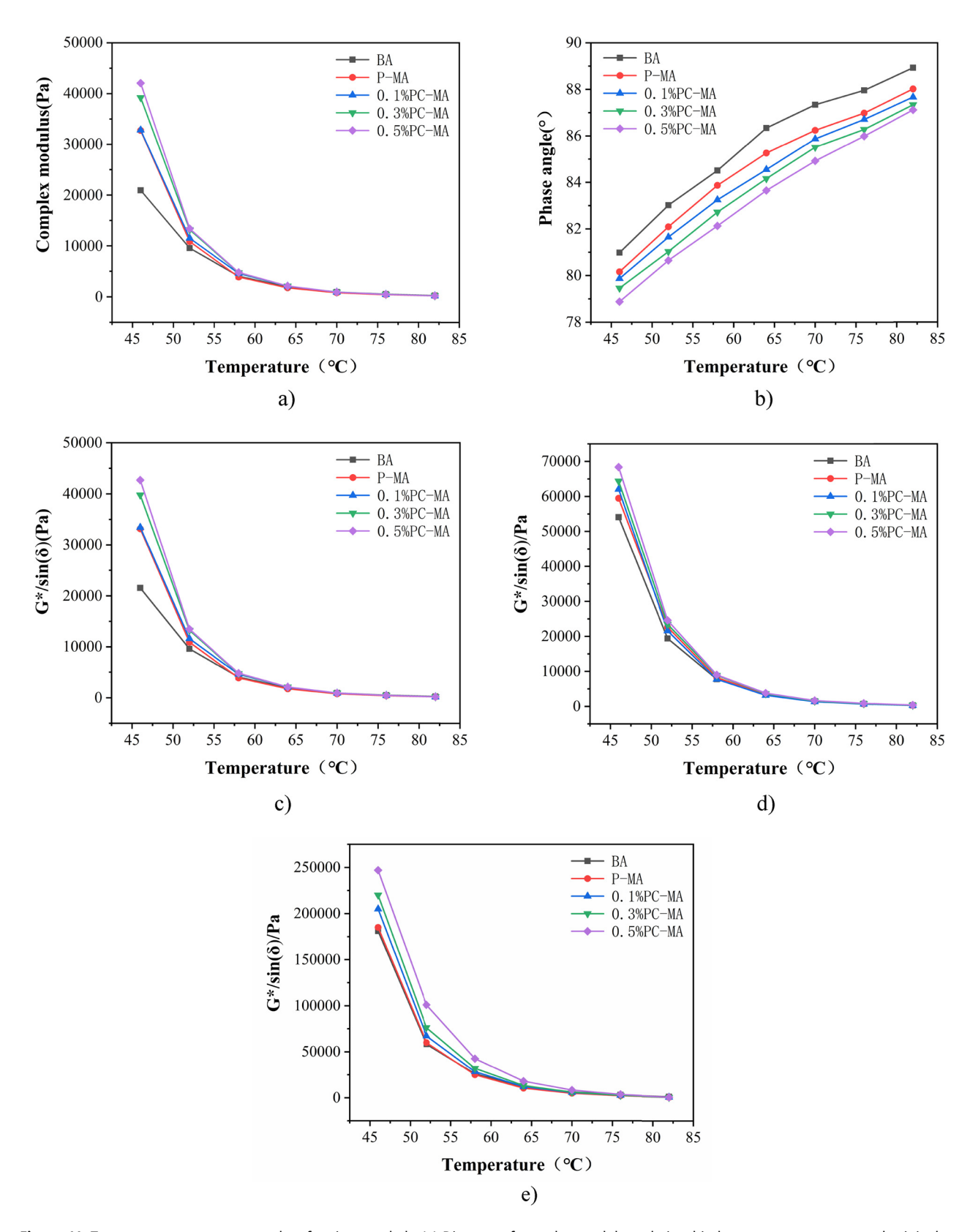


Figure 11: Temperature sweep test results of various asphalt. (a) Diagram of complex modulus relationship between temperature and original asphalt, (b) diagram of phase angle relationship between temperature and original asphalt, (c) temperature–original asphalt rutting factor relationship, (d) temperature–RTFOT asphalt rutting factor relationship, and (e) temperature–PAV asphalt rutting factor relationship.

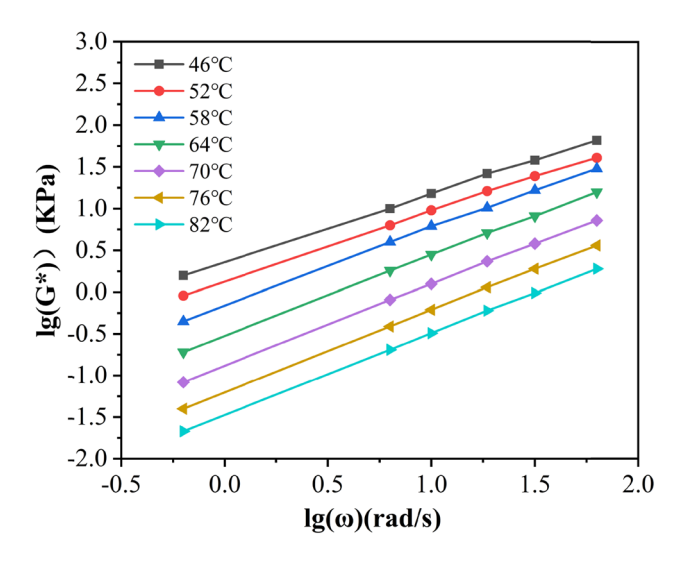
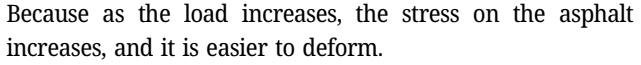


Figure 12: Complex modulus—angular frequency relationship of P-MA asphalt at different temperatures.



According to Figure 15, $J_{\rm nr}$ values increase with the temperature under two stress conditions, and the value of heavy load stress is greater than that of light load stress under the same temperature condition. Under the same external conditions, the $J_{\rm nr}$ value of different asphalts is the highest value of BA, and with the addition of modifier, $J_{\rm nr}$ value gradually decreases, suggesting that modifier improves the anti-deformation ability of asphalt. It is found that the $J_{\rm nr}$ value of PC-MA is lower than that of P-MA,

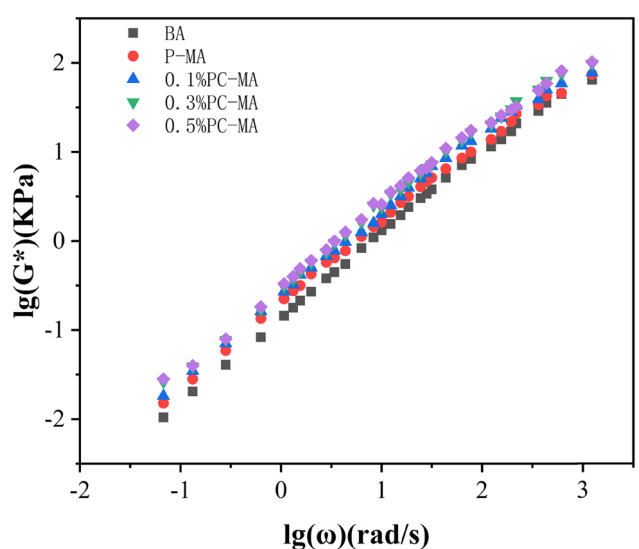


Figure 13: Main curves of various asphalts.

indicating that the addition of CFF further improves the rutting resistance of asphalt.

4.2 Low temperature rheological property

According to the test principle and test procedures of BBR, trabecular specimens with different asphalts such as BA, P-MA, 0.1%PC-MA, 0.3%PC-MA, and 0.5%PC-MA were prepared, and then BBR tests were carried out at -6, -12, and -18°C for different bituminous trabecular specimens. The

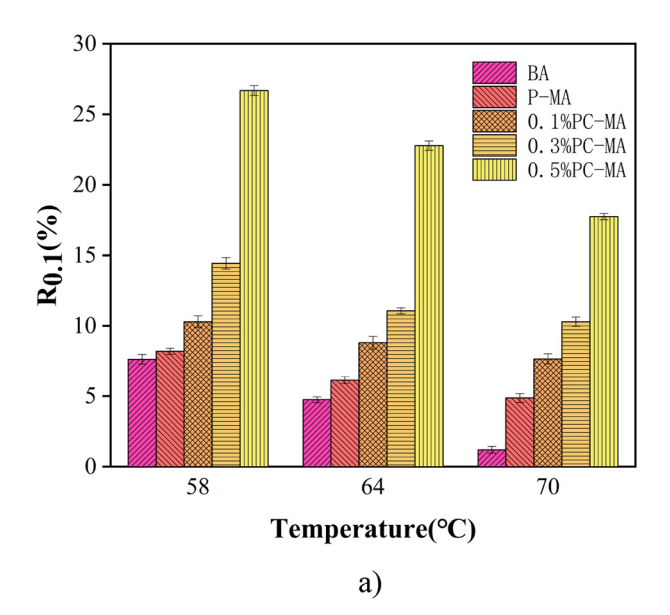
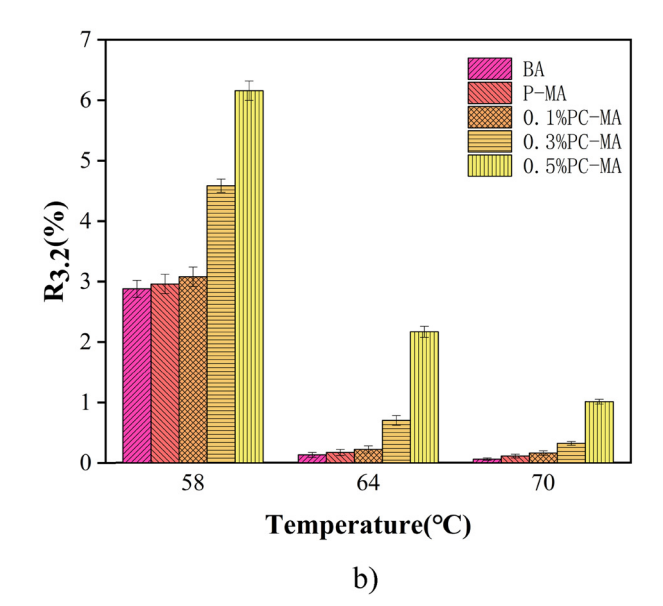
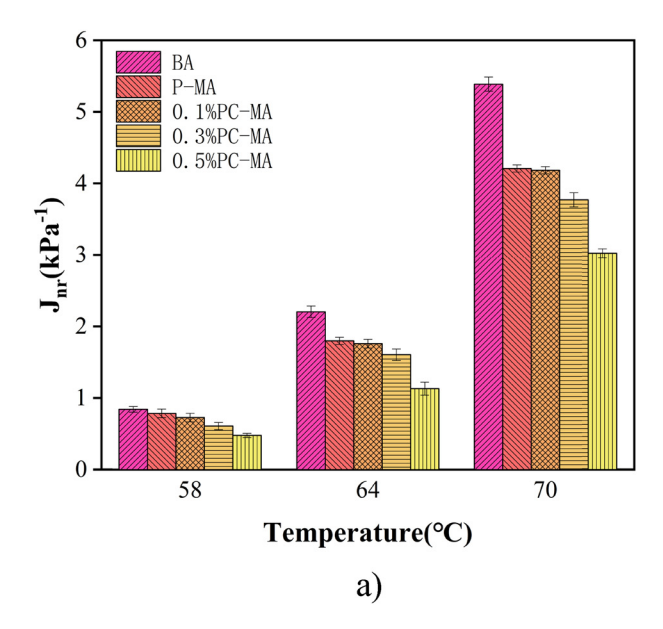


Figure 14: R of various asphalt. (a) 0.1 kPa and (b) 3.2 kPa.





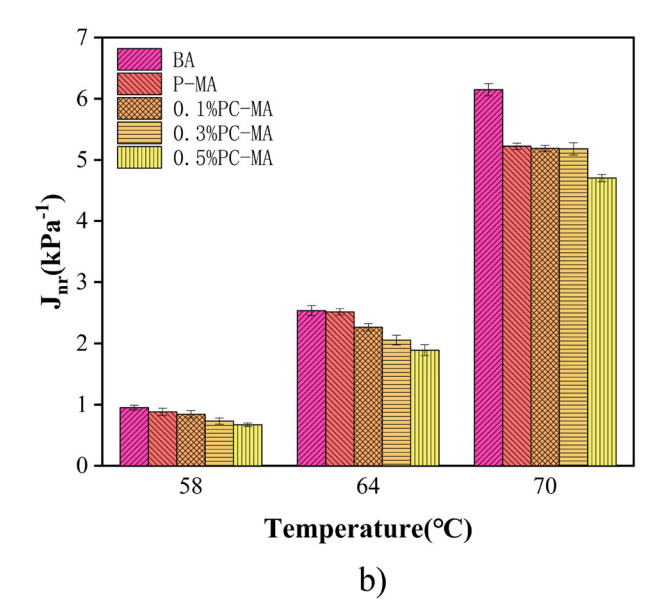


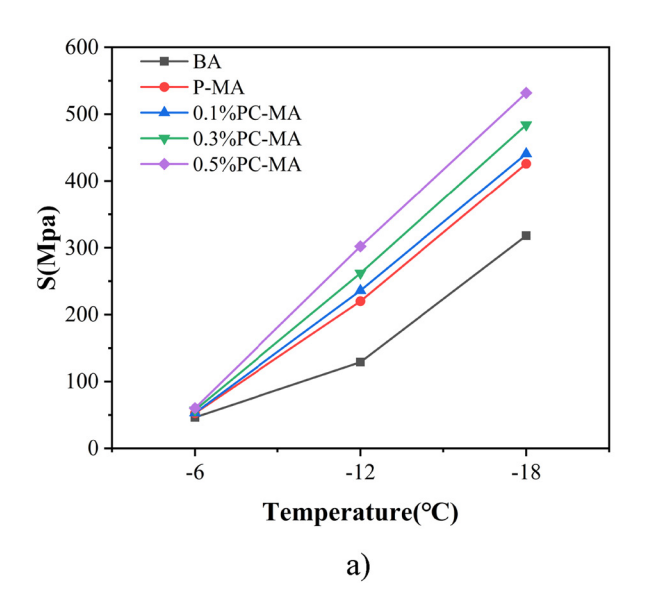
Figure 15: J_{nr} of various asphalts. (a) 0.1 kPa and (b) 3.2 kPa.

test results of S and m, two evaluation indexes, are presented in Figure 16.

According to Figure 16a, *S* increases rapidly with the decrease in the temperature. When the temperature drops, the asphalt becomes hard and brittle. According to the results of *S*, low-temperature performance of asphalt from good to bad is as follows: BA, P-MA, 0.1%PC-MA, 0.3%PC-MA, and 0.5%PC-MA, indicating that PCB and CFF affect asphalt low-temperature performance. Among them, the *S* of P-MA, 0.1%PC-MA, and 0.3%PC-MA asphalt is similar, suggesting that low dosage CFF does not affect PCB modified asphalt

performance. The S of asphalt should be less than 300 MPa, and the S of all kinds of asphalt meets the requirements at -6° C. However, the S of 0.5%PC-MA at -12° C exceeds the technical requirements. At -18° C, all kinds of asphalt S cannot meet the requirements. However, in most southern cities of China, the annual minimum temperature is about -10° C, and the S of 0.5% CFF does not meet the requirements, so the optimal dosage of CFF is 0.3%.

According to Figure 16b, the m decreases rapidly with the decrease in temperature, and its relaxation property at low temperature gradually deteriorates, resulting in the



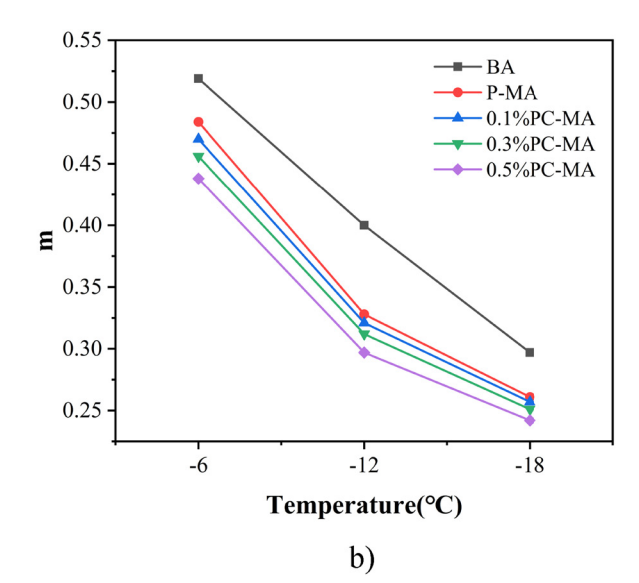


Figure 16: Relation between S and m at different temperatures. (a) S and (b) m.

decrease of its low temperature property. In terms of m, the low temperature properties from good to bad are as follows: BA, P-MA, 0.1%PC-MA, 0.3%PC-MA, and 0.5%PC-MA, and the results are consistent with those of S. At the same time, the m at -6°C meets the technical requirements, while the m of 0.5%PC-MA at -12°C is lower than the standard requirement of 0.3, making it unsuitable for pavement asphalt use. So, the maximum dosage of CFF is 0.3%.

4.3 Temperature sensitivity analysis

Based on the penetration results at different temperatures, linear fitting was carried out, and the coefficient A and constant term K were determined. After that, we calculated penetration index (PI) using Eq. (2). Results of different asphalt penetration degrees are presented in Table 10.

$$PI = \frac{20 - 500A}{1 + 50A}.$$
 (2)

It is evident from Table 10 that PI changes among different asphalts. As PI increases, asphalt becomes less temperature sensitive and external temperature has less influence. Among them, 0.3% PC-MA has the largest PI and external temperature has the least effect.

The lower the equivalent brittleness point $(T_{1.2})$ of asphalt, the better its low temperature cracking resistance. According to the A and K values in Table 10 combined with Eq. (3), the $T_{1.2}$ is a measure of the low-temperature cracking resistance of asphalt. The $T_{1.2}$ results are shown in Figure 17.

$$T_{1.2} = \frac{\lg 1.2 - K}{A}.$$
 (3)

In this case, $T_{1.2}$ is the temperature when the penetration is 1.2.

According to Figure 17, with the increase in CFF dosage, the $T_{1.2}$ decreases first and then increases. Among the different types of asphalt evaluated, it has been observed that asphalt containing 0.3%PC-MA exhibits the lowest $T_{1.2}$ value.

This indicates that this particular asphalt formulation demonstrates superior resistance to low temperature cracking, comparable to the effect of incorporating fibers into the mixture to enhance cracking resistance.

5 Micro structure characterization

A microscopic study examined the mechanism and effect of composite modification were analyzed through the microscopic test of BA, P-MA, and PC-MA, among which PC-MA was prepared under optimal parameters of composite-modified asphalt, 0.3%PC-MA.

5.1 Chemical groups

Based on FTIR results, we analyzed the changes in energy spectrum between different asphalt and the modification of asphalt additives. The FTIR results are shown in Figure 18.

According to the wavelength of the characteristic peak of asphalt in Figure 18, based on the characteristic peak of

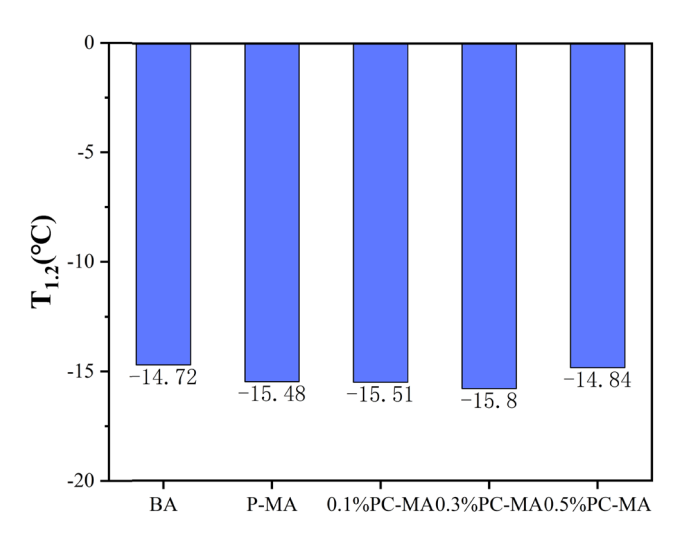


Figure 17: Different asphalt $T_{1,2}$.

Table 10: Results of different asphalt penetration

Asphalt type	Penetration (0.1 mm)			R ²	A	K	PI
	15°C	25°C	30°C				
BA	26.6	68.6	112.8	0.9998	0.0443	0.77354	-0.6832
P-MA	20.8	55.3	96.6	0.9968	0.0416	0.7232	-0.2597
0.1%PC-MA	20.1	54.5	95.1	0.9981	0.0413	0.7198	-0.2121
0.3%PC-MA	19.2	52.8	92.8	0.998	0.0409	0.7256	-0.1478
0.5%PC-MA	18.6	51.1	90.1	0.9977	0.0413	0.6921	-0.2121

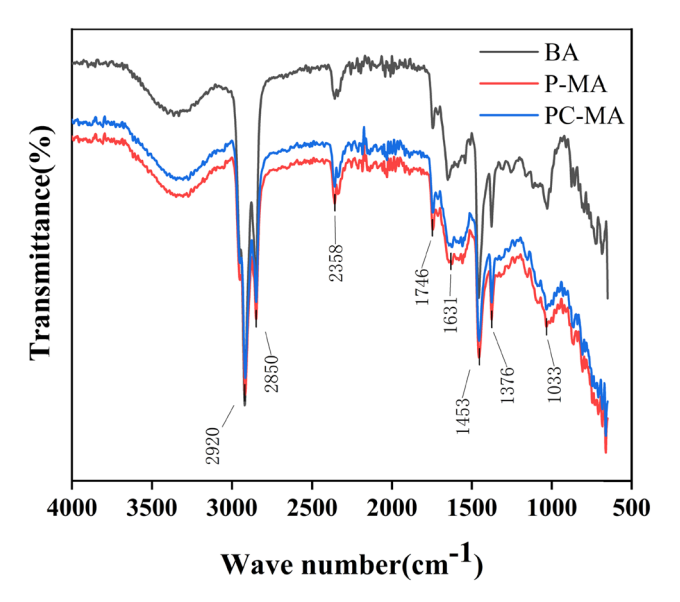


Figure 18: FTIR of different asphalts.

2,920 cm⁻¹, CH₂ alkane is mainly characterized by anti-symmetric stretching vibrations. At the sharp characteristic peak of 2,850 cm⁻¹, it is CH₂ alkane's symmetric stretch vibration. The characteristic peak at 2,358 cm⁻¹ is not the absorption peak generated by asphalt, but the absorption peak generated by the background irradiation during the infrared spectrum test. The vibration intensity of CO2 in the air is high, and the air dosage in asphalt is low, so the characteristic peak of asphalt functional group cannot be shown. In the analysis of asphalt functional group, this characteristic peak can be ignored. At the characteristic peak of 1,746 cm⁻¹, it is the vibration of ester carbonyl group in C=0 carbonyl group and the stretching vibration of saturated fatty acid ester. At the characteristic peak of 1.631 cm⁻¹, it is C=C olefin stretching vibration. Because it is a central symmetric functional group with low vibration intensity, the characteristic peak is difficult to distinguish. We also have C=O carbonyl amido-carbonyl stretching vibration. At the characteristic peak 1,453 cm⁻¹, the antisymmetric bending vibration of methyl CH3 is generated. At the right, 1,376 cm⁻¹ characteristic peak, methyl CH₃ is generated by symmetric bending vibration. At the characteristic peak of 1,033 cm⁻¹, it is the stretching vibration of S=O group sulfoxide R¹-SO-R² group. To sum up, methyl and methylene in asphalt have obvious recognition, and the substances in asphalt are complex.

According to the frequency of asphalt characteristic peaks in Figure 18, the transmittance of P-MA and PC-MA is lower than that of BA, but the transmittance of them is close to each other [40]. Compared with the BA, the spectrum of P-MA has little change, and no new absorption peak appears in the whole functional group region. It is inferred that there is no chemical reaction between PCB and BA, indicating that the physical reaction plays a major role between PCB and BA, which is consistent with the research conclusion of Mo et al. [41]. Similarly, the relationship between CFF and PCB modified asphalt also belongs to physical modification.

5.2 Dispersibility analysis

The compatibility of asphalt additives and uniformity of modifier distribution were examined using a fluorescence microscope. The result is shown in Figure 19.

Figure 19a shows the FM result of BA. It can be seen from Figure 19b that P-MA can be evenly dispersed in asphalt, indicating that PCB has good compatibility with asphalt. However, the size of PCB particles is not consistent, and the phenomenon of clumping exists. The reason is that the molecular force between PCB is large, resulting in the aggregation of smaller PCB particles, which is consistent with the research conclusion of Xie et al. [40]. According to Figure 19c, compared with P-MA, the fluorescence results show a bright feather shape after the addition of CFF, which is due to the different degrees of light absorption and reflection of CFF and the PCB. Meanwhile, PCB can still be evenly dispersed in asphalt after adding CFF to P-MA, and the addition of CFF does not produce a large amount of adsorption of PCB.

6 Route performance verification

PC-MA asphalt was prepared using optimal combination parameters. Three types of asphalt mixtures, BA, P-MA, and PC-MA, were designed and their pavement performance was evaluated. To facilitate the comparison of asphalt performance, identical aggregates and gradations were employed in the production of the three asphalt mixtures. In order to eliminate the influence of grading factors on the pavement performance of asphalt mixtures and highlight the comparability of asphalt mixtures with different properties, the median value of AC-13 grading was uniformly adopted for mixture grading, as shown in Table 11. Marshall test showed that the optimal asphalt aggregate ratio was 4.6% for BA mixture, 4.8% for P-MA mixture, and 4.7% for PC-MA mixture. In accordance with the Chinese standard JTG E20-2011, a study was conducted to assess the high and lowtemperature performance of BA, P-MA, and PC-MA mixture with an optimal asphalt aggregate ratio using the wheel track test T0719 and low-temperature bending test T0715, based on dynamic stability and Flexural strain. To further evaluate the water stability of the BA, P-MA, and PC-MA mixture, the

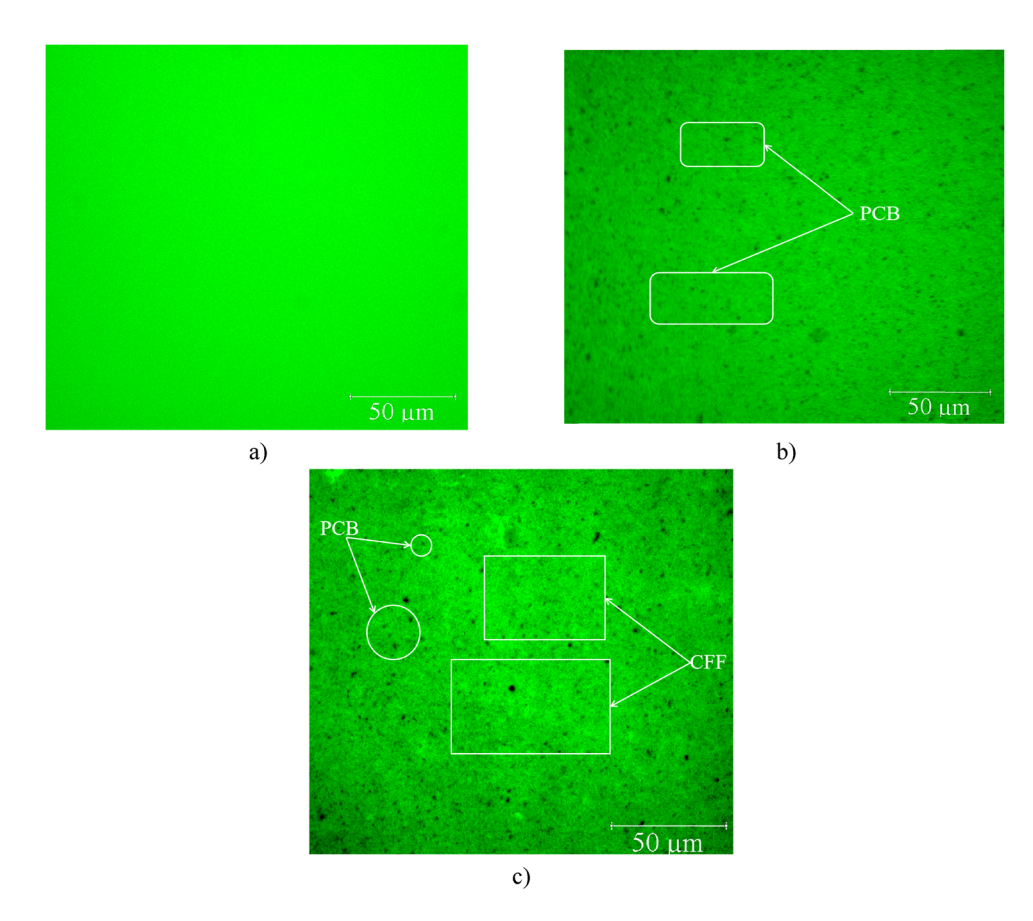


Figure 19: FM of various types of asphalt. (a) BA, (b) P-MA, and (c) PC-MA.

Table 11: Mineral grading of AC-13 asphalt mixture

				The fo	ollowing siev	/e (mm) pas	ss rate (%)			
Screen size (mm)	16	13.2	9.5	4.75	2.36	1.18	0.6	0.3	0.15	0.075
Upper limit of grading	100	100	80	53	40	27	19	15	10	8
Lower limit of grading	100	90	68	42	28	15	10	7	5	4
Synthetic grading	100	95	74	47.5	34	21	14.5	11	7.5	6

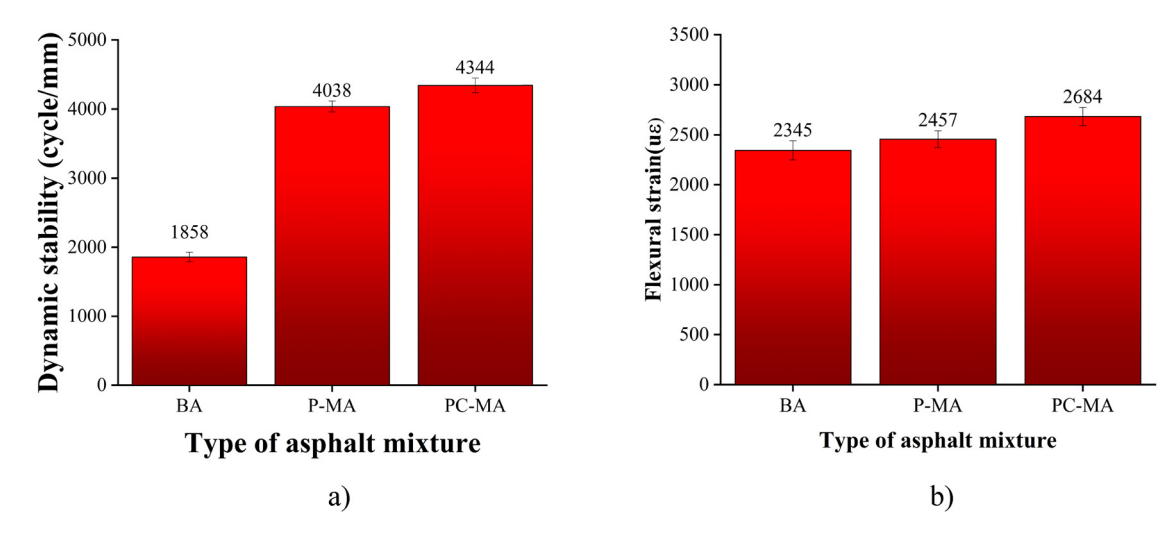
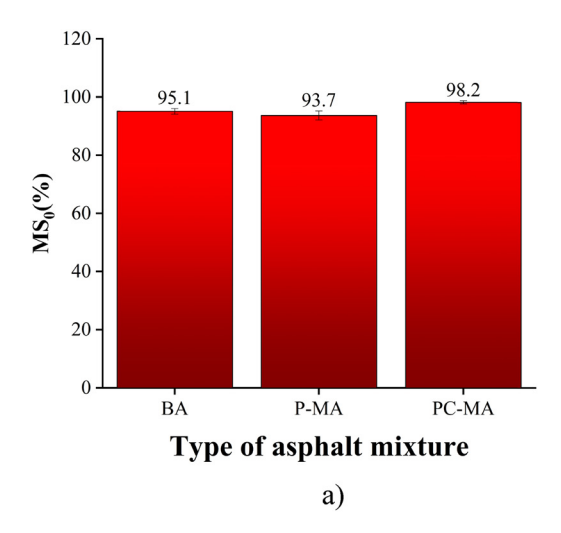


Figure 20: Verification results. (a) High-temperature performance and (b) low-temperature performance.



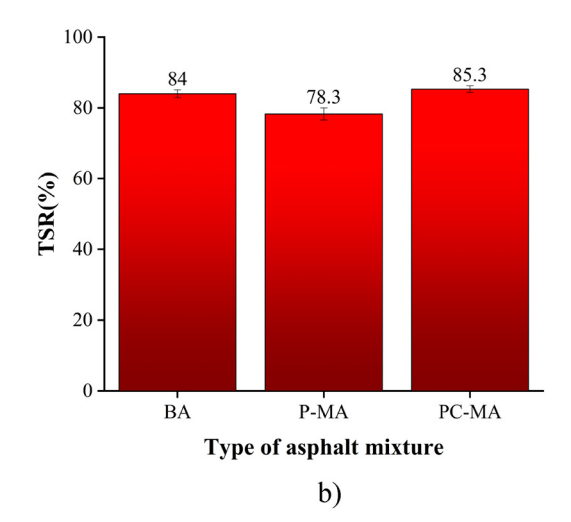


Figure 21: Verification results of water stability. (a) MS₀ and (b) TSR.

immersion Marshall test method T0709 and freeze-thaw splitting test method T0729 were employed, with a focus on residual Marshall stability (MS_0) and splitting tensile strength ratio. The road performance results are shown in Figures 20 and 21.

According to Figure 20a, PCB and CFF can improve the high-temperature performance of asphalt, and the addition of CFF to PCB-modified asphalt further improves the dynamic stability of PCB-modified asphalt. As can be seen from Figure 20b, the addition of PCB and CFF can improve the low-temperature performance of asphalt, while the single PCB asphalt has little improvement in low-temperature performance, while the composite addition of PCB and CFF can significantly increase the maximum flexural strain.

Figure 21 illustrates a pronounced decline in water stability of asphalt mixture upon incorporation of PCB. Addition of PCB, a granular substance, is intended to increase the stiffness of asphalt and diminish its viscoelasticity. However, the exposure of the modified asphalt mixture to environmental conditions, such as rainfall and wheel loads, causes a loss of adhesion between the asphalt and aggregate, which in turn leads to a reduction in water stability. By contrast, the introduction of CFF bolsters the binding capacity of asphalt, curtails the chances of asphaltaggregate separation, and ultimately elevates the water stability of the P-MA mixture.

7 Conclusion

The optimal preparation parameters for PC-MA were determined through a BBD experiment and regression analysis using RSM. High-temperature and low-temperature rheological

properties of BA, P-MA, and PC-MA were tested. The microscopic performance and the chemical groups of PC-MA were analyzed using infrared spectroscopy and FM. Finally, high temperature and low temperature performance tests, as well as water stability tests, were conducted on BA, P-MA, and PC-MA asphalt mixtures. The following conclusions were drawn:

1) The optimized parameters for the PCB/CFF composite-modified asphalt were obtained through BBD test of RSM. The reliability of the optimal parameters was verified. The PCB dosage in PCB/CFF-modified asphalt was found to be higher than that in single PCB-modified asphalt. The results show that CFF can increase the amount of PCB in asphalt and maintain good asphalt properties.

2) The addition of PCB and CFF enhanced the high temperature performance and anti-aging performance of asphalt, and the rheological properties at high temperature increased gradually with the increase of CFF dosage. Too short or too long CFF length has no obvious effect on the low temperature performance of asphalt, and even reduces the low temperature performance of asphalt, so moderate CFF length should be selected. The spatial network structure of CFF plays a good role in improving the high temperature performance of PCB modified asphalt.

3) The rheological properties at high and low temperatures of 0.3%PC-MA were proven to be the best, and the low-temperature rheological property of PC-MA decreased with the increase in CFF dosage as evaluated by BBR test. The high amount of CFF will have a negative effect on the low-temperature performance of asphalt, so the amount of CFF should be controlled reasonably.

4) PCB and CFF were physically blended with asphalt without chemical reaction, and they were well compatible with asphalt and evenly distributed in asphalt as analyzed by infrared spectroscopy and FM.

5) The addition of CFF can significantly improve the high-temperature and low-temperature performances, as well as water stability of PCB-modified asphalt mixtures. The results show that the high toughness, low density, and structure characteristics of CFF in space network can improve the road performance of PCB-modified asphalt mixture. Therefore, the PCB/CFF composite-modified asphalt is a promising alternative for high performance asphalt.

Acknowledgments: This work was supported by The Science and Technology Project of the Department of Transportation of Jiangxi Province (No. 2023H0025) and The scientific research fund of Hunan Provincial Education Department (No. 22B0984).

Funding information: The Science and Technology Project of the Department of Transportation of Jiangxi Province (No. 2023H0025); The scientific research fund of Hunan Provincial Education Department (No. 22B0984).

Author contributions: Chuangmin Li: methodology, investigation, data curation, software, validation, writing – review and editing, funding acquisition; Zhuangzhuang Li: conceptualization, methodology, data curation, writing – original draft, and writing – review and editing; Youwei Gan: writing – review and editing, resources, data curation, and software; Qinhao Deng: methodology, writing – review and editing, resources, and validation. All authors have accepted responsibility for the entire content of this manuscript and approved its submission.

Conflict of interest: The authors state no conflict of interest.

Data availability statement: The datasets generated and/ or analysed during the current study are available from the corresponding author on reasonable request.

References

- [1] Thomas, B. S., R. C. Gupta, P. Kalla, and L. Cseteneyi. Strength, abrasion and permeation characteristics of cement concrete containing discarded rubber fine aggregates. *Construction and Building Materials*, Vol. 59, No. May 30, 2014, pp. 204–212.
- [2] Xu, J., J. Yu, J. Xu, C. Sun, W. He, J. Huang, and G. Li. High-value utilization of waste tires: A review with focus on modified carbon black from pyrolysis. *Science of the Total Environment*, Vol. 742, 2020, id. 140235.
- [3] Lin, Y. T., F. Y. Kao, S. H. Chen, M. Y. Wey, and H. H. Tseng. A facile approach from waste to resource: Reclaimed rubber-derived membrane for dye removal. *Journal of the Taiwan Institute of Chemical Engineers*, Vol. 112, 2020, pp. 112–295.

- [4] Liu, H., X. Wang, and D. Jia. Recycling of waste rubber powder by mechano-chemical modification. *Journal of Cleaner Production*, Vol. 245, 2020, id. 118716.
- [5] Yung, W. H., L. C. Yung, and L. H. A. Hua. Study of the durability properties of waste tire rubber applied to self-compacting concrete. *Construction & Building Materials*, Vol. 41, 2013, pp. 665–672.
- [6] Li, L., S. Ruan, and L. Zeng. Mechanical properties and constitutive equations of concrete containing a low volume of tire rubber particles. *Construction and Building Materials*, Vol. 70, 2014, pp. 291–308.
- [7] Wu, X., S. Wang, and R. Dong. Lightly pyrolyzed tire rubber used as potential asphalt alternative. *Construction and Building Materials*, Vol. 112, 2016, pp. 623–628.
- [8] Quek, A. and R. Balasubramanian. Liquefaction of waste tires by pyrolysis for oil and chemicals – A review. *Journal of Analytical and Applied Pyrolysis*, Vol. 101, 2013, pp. 1–16.
- [9] Feng, Z., W. Rao, C. Chen, B. Tian, X. Li, P. Li, and Q. Guo. Performance evaluation of bitumen modified with pyrolysis carbon black made from waste tyres. *Construction and Building Materials*, Vol. 111, 2016, pp. 495–501.
- [10] Wang, H., G. Lu, S. Feng, X. Wen, and J. Yang. Characterization of bitumen modified with pyrolytic carbon black from scrap tires. *Sustainability*, Vol. 11, No. 6, 2019, id. 1631.
- [11] Tacettin, G., A. Perviz, and A. Taner. Effect of carbon black on the high and low temperature properties of bitumen. *International Journal of Civil Engineering*, Vol. 16, No. 2, 2018, pp. 1–12.
- [12] Liu, X., S. Wu, Q. Ye, Q. Jian, and L. Bo. Properties evaluation of asphalt-based composites with graphite and mine powders. Construction & Building Materials, Vol. 22, No. 3, 2008, pp. 121–126.
- [13] Abdulfattah, O., I. H. Alsurakji, A. El-Qanni, M. Samaaneh, M. Najjar, R. Abdallah, et al. Experimental study on optimum additive content of pyrolytic carbon black asphalt mixture. *Journal of Changsha University of Science & Technology (Natural Science)*, Vol. 19, No. 4, 2022, pp. 161–170.
- [14] Kakade, B. V., A. M. Reddy, and S. K. Reddy. Effect of aging on fatigue performance of hydrated lime modified bituminous mixes. *Construction and Building Materials*, Vol. 113, 2016, pp. 1034–1043.
- [15] Xin, G., W. Jiayu, and X. Feipeng. Sponge city strategy and application of pavement materials in sponge city. *Journal of Cleaner Production*, Vol. 303, No. 1, 2021, id. 127022.
- [16] Cong, P., P. Xu, and S. Chen. Effects of carbon black on the antiaging, rheological and conductive properties of SBS/asphalt/ carbon black composites. *Construction and Building Materials*, Vol. 52, 2014, pp. 306–313.
- [17] Abhinay, K., C. Rajan, and K. Ankush. Characterization of thermal storage stability of waste plastic pyrolytic char modified asphalt binders with sulfur. *PloS One*, Vol. 16, No. 3, 2021, id. 0248465.
- [18] Qiang, X., L. Lei, and C. Yi-jun. Study on the action effect of pavement straw composite fiber material in asphalt mixture. *Construction and Building Materials*, Vol. 43, 2013, pp. 293–299.
- [19] Li, Z., X. Zhang, C. Fa, Y. Zhang, J. Xiong, and H. Chen. Investigation on characteristics and properties of bagasse fibers: Performances of asphalt mixtures with bagasse fibers. *Construction and Building Materials*, Vol. 248, No. 6, 2020, id. 118648.
- [20] Zhang, X., X. Sheng, T. Miao, K. Yao, and D. Yao. Laboratory investigation on the use of bamboo fiber in asphalt mixtures for enhanced performance. *Arabian Journal for Science and Engineering*, Vol. 44, No. 5, 2019, pp. 4629–4638.
- [21] Zhijie, T., G. Youwei, Y. Ting, et al. Study on betel nut fiber enhancing water stability of asphalt mixture based on response

- surface method. *Case Studies in Construction Materials*, Vol. 16, 2022, id. e00870.
- [22] Mu, B., F. Hassan, and Y. Yang. Controlled assembly of secondary keratin structures for continuous and scalable production of tough fibers from chicken feathers. *Green Chemistry*, Vol. 22, No. 5, 2020, pp. 1726–1734.
- [23] Tesfaye, T., B. Sithole, D. Ramjugernath, and T. Mokhothu. Valorisation of chicken feathers: Characterisation of thermal, mechanical and electrical properties. Sustainable Chemistry and Pharmacy, Vol. 9, 2018, pp. 27–34.
- [24] Tesfaye, T., B. Sithole, D. Ramjugernath, and V. Chunilall. Valorisation of chicken feathers: Characterisation of physical properties and morphological structure. *Journal of Cleaner Production*, Vol. 149, 2017, pp. 349–365.
- [25] Ab, S. E. W. and F. S. O. Che. Mechanical properties of concrete added with chicken rachis as reinforcement. *Applied Mechanics and Materials*, Vol. 147, No. 147–147, 2011, pp. 37–41.
- [26] Rivera-Armenta, J. L., B. A. Salazar-Cruz, M. Y. Chávez-Cinco, A. B. Morales-Cepeda, and S. Zapién-Castillo. Influence of chicken feather on the rheological properties and performance of modified asphalts. *Construction and Building Materials*, Vol. 264, 2020, pp. 120128–120139.
- [27] Dalhat, M. A., S. A. Osman, A. A. A. Alhuraish, F. K. Almarshad, S. A. Qarwan, and A. Y. Adesina. Chicken Feather fiber modified hot mix asphalt concrete: Rutting performance, durability, mechanical and volumetric properties. *Construction and Building Materials*, Vol. 239, 2020, id. 117849.
- [28] Youwei, G., L. Chuangmin, C. Anqi, L. Yuan, and W. Shaopeng. A model of pyrolysis carbon black and waste chicken feather using a response surface method in hot-mix asphalt mixtures. *Journal of Materials in Civil Engineering*, Vol. 34, 2022, id. 11.
- [29] Colunga-Sánchez, L. M., B. A. Salazar-Cruz, J. L. Rivera-Armenta, A. B. Morales-Cepeda, C. E. Ramos-Gálvan, and M. Y. Chávez-Cinco. Evaluation of chicken feather and styrene-butadiene/chicken feather composites as modifier for asphalts binder. *Applied Sciences*, Vol. 9, No. 23, 2019, id. 5188.
- [30] Loganathan, M., S. Dinesh, V. Vijayan, M. Ranjithkumar, and S. Rajkumar. Experimental investigation of tensile strength of fiber reinforced polyester by using chicken feather fiber. *Journal of New Materials for Electrochemical Systems*, Vol. 23, No. 1, 2020, pp. 16–20.
- [31] Park, P., S. El-Tawil, S. Y. Park, and A. E. Naaman. Cracking resistance of fiber reinforced asphalt concrete at −20°C. *Construction and Building Materials*, Vol. 81, 2015, pp. 47–57.

- [32] Zhang, X., Y. Zhang, Y. Wu, and P. Xia. Viscoelastic equivalent creep behavior and its influencing factors of basalt fiber-reinforced asphalt mixture under indirect tensile condition. *Advances in Materials Science and Engineering*, Vol. 2021, No. 1, 2021, pp. 1–13.
- [33] Yang, Y. and Y. Cheng. Preparation and performance of asphalt compound modified with waste crumb rubber and waste polyethylene. *Advances in Materials Science and Engineering*, Vol. 2016, 2016, pp. 1–6.
- [34] Li, C., F. Ning, and Y. Li. Effect of carbon black on the dynamic moduli of asphalt mixtures and its master curves. Frontiers of Structural and Civil EngineeringACS nano, Vol. 13, No. 4, 2019, pp. 918–925.
- [35] Omranian, S. R., M. O. Hamzah, J. Valentin, and M. R. Hasan. Determination of optimal mix from the standpoint of short term aging based on asphalt mixture fracture properties using response surface method. *Construction & Building Materials*, Vol. 179, No. Aug 10, 2018, pp. 35–48.
- [36] Tan, R., J. Liu, M. Li, J. Huang, J. Sun, and H. Qu. Performance optimization of composite modified asphalt sealant based on rheological behavior. *Construction & Building Materials*, Vol. 47, 2013, pp. 799–805.
- [37] Zhang, P., Y. C. Cheng, J. L. Tao, and Y. B. Jiao. Molding process design for asphalt mixture based on response surface methodology. *Journal of Materials in Civil Engineering*, Vol. 28, No. 11, 2016, id. 0001640.
- [38] Hamzah, O. M., B. Golchin, and D. Woodward. A quick approach for rheological evaluation of warm asphalt binders using response surface method. *Journal of Civil Engineering and Management*, Vol. 23, No. 4, 2017, pp. 475–486.
- [39] Li, C., B. Peng, X. Gan, and W. Yang. Indoor test research on road performance of TPCB modified asphalt mixture prepared by dry and wet method. *Journal of Changsha University of Science & Technology (Natural Science)*, Vol. 19, No. 2, 2022, pp. 49–60.
- [40] Xie, X., T. Hui, Y. Luo, H. Li, G. Li, and Wang Z. Research on the properties of low temperature and anti-UV of asphalt with Nano-ZnO/Nano-TiO₂/copolymer SBS composite modified in high-altitude. Areas Advances in Materials Science and Engineering, Vol. 2020, No. 5, 2020, pp. 1–15.
- [41] Shi, J., W. Chen, X. Mo, J. Liu, X. He, and K. Yang. Experimental investigation of bituminous plug expansion joint materials containing high content of crumb rubber powder and granules. *Materials & Design*, Vol. 37, 2012, pp. 137–143.